AD-A106 116 ATOMIC ENERGY RESEARCH ESTABLISHMENT HARWELL (ENGLAND) F/G 11/6
THE INFLUENCE OF WATER CHEMISTRY ON FATIGUE CRACK PROPAGATION I--ETC(U)
JUN 81 P M SCOTT, A E TRUSWELL
UNCLASSIFIED AERE-R-10201 NL

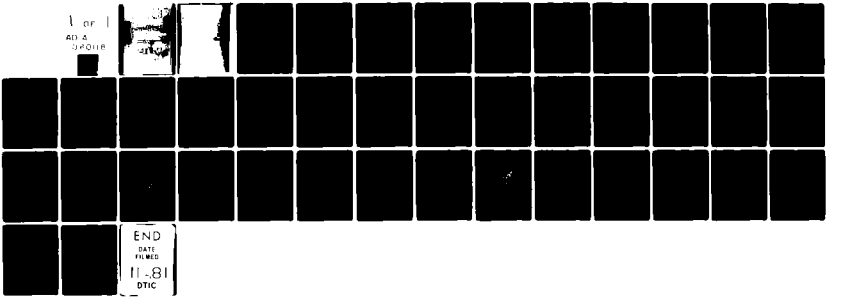

END
DATE FILMED
11-81
DTIC

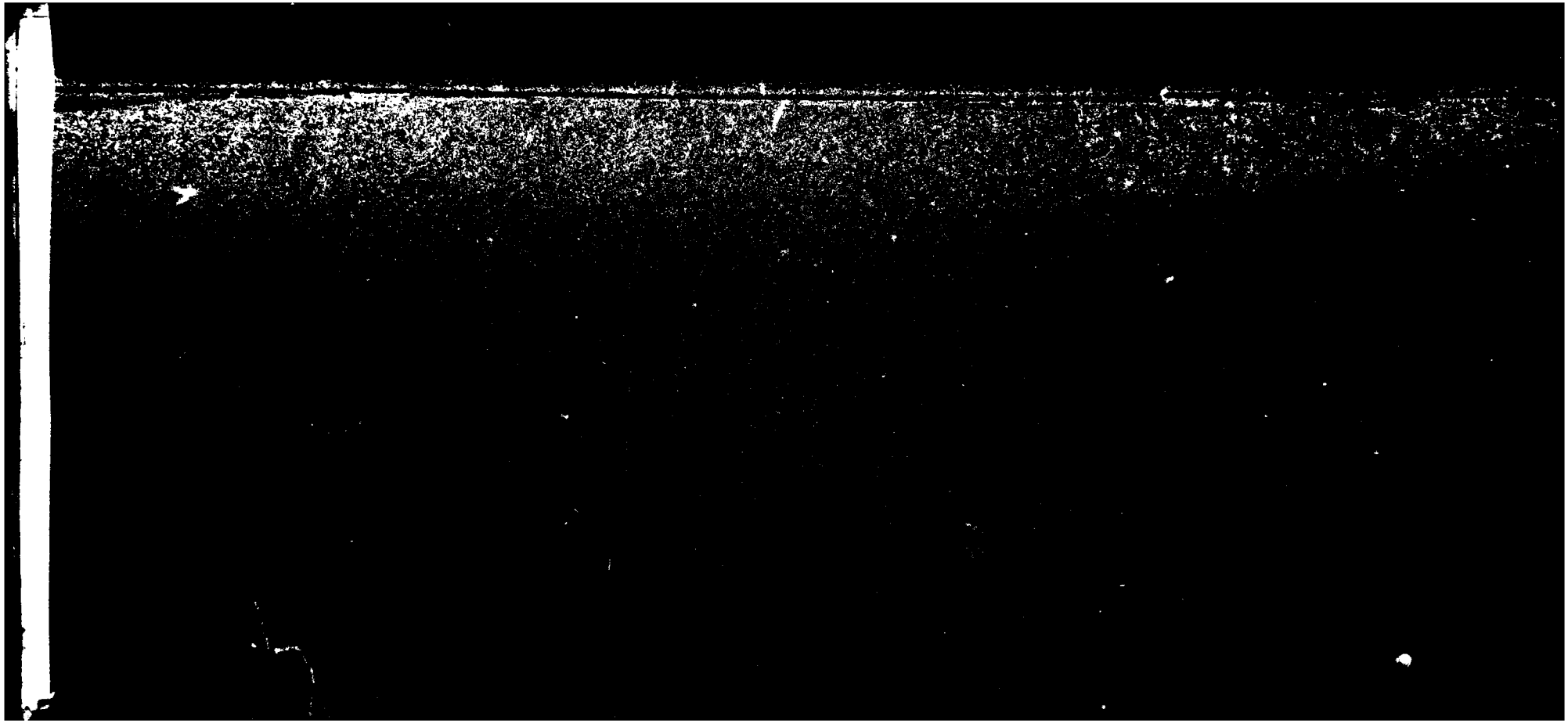

AERE-R 10201

The Influence of Water Chemistry on Fatigue Crack Propagation in LWR Pressure Vessel Steels

P.M. Scott and A.E. Truswell

Abstract

The results of an experimental programme designed to obtain corrosion fatigue crack growth data for pressure vessel steels are described. The work has concentrated on assessing the influence of various water chemistry variables possible in PWR or BWR primary coolants on fatigue crack propagation rates in A533-B steel.

At a low cyclic frequency, 0.0167 Hz, the only variable found to have a significant effect on crack growth rates when compared with an inert helium environment at the same temperature, 288°C, is the dissolved oxygen concentration at levels in excess of 100 ppb. However, the effect of the oxygenated water on crack growth is observed to decay rapidly with time of exposure and this is attributed to passivation of surfaces previously created in a short period of time by high frequency cycling.

At higher cyclic frequencies of 1.0 Hz or greater, periods of constant crack growth rate independent of the applied cyclic stress intensity factor have been observed in all the aqueous environments examined. The reaon for this behaviour is believed to be the occurrence of a form of strain rate sensitive stress corrosion cracking superimposed on normal fatigue behaviour. A mechanistic model based on this propostion is developed and is used to explain how the electrochemical conditions within the experimental rigs of different laboratories can influence the range of frequency and stress ratio over which the stress corrosion phenomenon can occur. It is suggested that this mechanism accounts for apparent laboratory to laboratory disagreements from nominally the same corrosion fatigue experiments.

Materials Development Division,
A.E.R.E., Harwell.

June 1981

HL.81/1792 (C21)

Contents

Tables

Illustrations

Illustrations (continued)

1. INTRODUCTION

It is now over ten years since Kondo and his co-workers first reported that a typical (simulated) Boiling Water Reactor (BWR) environment could cause fatigue cracks to grow much faster in reactor pressure vessel steels than in the same steels exposed to an inert environment[1]. Subsequently, it was shown that a Pressurized Water Reactor (PWR) simulated primary circuit coolant could also cause very large increases in fatigue crack propagation rates[2]. Since then, a considerable international effort has been mounted to determine the influence of a large number of metallurgical and water chemistry variables which could possibly affect the rate of corrosion fatigue crack growth in reactor pressure vessel steels. Ultimately, a realistic and safe code of practice is required to enable the growth of any defect, which might be found as a result of in-service inspection and which might also be exposed to the primary coolant, to be quantitatively assessed.

The complexity of the necessary experimental equipment required to simulate LWR coolants, typically at 300°C and up to 17 MPa pressure, and the extremely time consuming nature of the experiments carried out at very low cyclic frequencies has dictated a comparatively slow rate of progress. Some confusing and apparent disagreements between the results from different laboratories have also been disclosed. In this paper, we describe the results of the UKAEA programme, which has, initially, concentrated on measuring the influence of various water chemistry variables while using comparatively few heats of A533-B plate pressure vessel steel. A mechanistic model based on the results is described which, it is believed, goes a long way towards explaining the anomalies which have appeared between the results of different laboratories, and points the way to those electrochemical conditions it is necessary to avoid in order to prevent unusually fast corrosion fatigue crack propagation rates in reactor pressure vessel steels.

2. EXPERIMENTAL

The experimental rig consists of four independent high pressure, high temperature water loops, each connected to individual autoclaves

which contain the fatigue specimens. A line drawing of the water recirculation loops and a cut-away drawing of the specimen assembly within the autoclaves is shown in Figure 1.

The feedwater to each of the recirculating loops can be varied over a wide specification of either PWR primary circuit water, BWR water or pure water; Table 1. The feedstock is de-ionised, de-oxygenated water with a conductivity typically of 0.08 $\mu S\ cm^{-1}$ and unmeasurable oxygen content, i.e. $<$10 ppb. For BWR water chemistry, a small portion of the feedstock is fully oxygenated at $\sim$0.5 bar oxygen pressure (or by additions of hydrogen perioxide), and then mixed in the appropriate proportions with deoxygenated water to give the desired oxygen content. In this mode of operation the blow-down water from each high pressure loop is run to waste. For PWR primary water, the appropriate concentrations of boric acid and lithium hydroxide are added to a mixing tank which is pressurised to $\sim$ 1.5 bar with either helium or hydrogen. The blowdown water from each loop in the PWR mode is returned to the mixing tank via a Potter column to provide continuous deoxygenation and lithiated and borated cation and anion resins to remove all ionic dissolved impurities other than lithium and borate ions.

The high pressure recirculating water loops can operate up to 300°c and 16 MPa pressure at a recirculation rate of $\sim$40 litres/ minute. The feedwater is metered in by a double diphragm, positive displacement pump at typically 20 to 40 litres/hour and is matched by an equivalent blowdown rate through a back pressure regulator. Thus about 1% of the recirculating flow is blown down on each water circuit. Water sampling points on the feed and bleed water flows are available for wet chemistry analysis. Dissolved gases can also be removed from these sample flows by a gas stripper and are then analysed by gas chromatography.

The fatigue specimens for this work were 25 or 50 mm thick compact tension specimens cut from A533-B plate steel with one of the three orientations shown in Figure 2. The steel compositions and mechanical properties are shown in Table 2. The fatigue crack lengths in the specimens were determined in-situ from measurements of the crack mouth

opening displacement using an encapsulated, linearly variable, displacement transducer. An on-line computer calculated the crack length from a calibration polynomial relating crack opening displacement divided by the applied load to crack length. This relation was determined in calibration experiments at 288°C in an inert helium environment[3]. Pre-cracking of the specimens was normally carried out in situ at the operating temperature and pressure over about eight hours. Step load reduction to the desired load range was followed by cyclic frequency reduction to the required frequency.

3. RESULTS

A series of experiments were carried out initially to establish an inert environment (helium gas) fatigue crack propagation base-line against which the subsequent corrosion fatigue results could be compared. These results and those for each water chemistry examined are described under individual sub-headings below.

3.1 Helium gas at 288°C

Compact tension specimens, 50 mm thick, all with L-S orientation manufactured from cast C8938 (Table 2) were used for these experiments. The results for sine and triangle waveshapes with cyclic frequencies in the range 10 Hz to 0.0167 Hz (1 cycle per minute) and stress ratios, R, (the minimum cyclic stress divided by the maximum cyclic stress) in the range 0.2 to 0.7 are shown in Figure 3. It can be seen that the mean slope of the results on the double logarithmic scales on Figure 3 is less than that given by the current ASME Section XI Appendix A code[4] such that the code line is non-conservative at values of ΔK less than 50 MPa $\sqrt{m}$. The practical significance of this is not very great[5] but for safe predictions of dry crack growth an adequate upper bound to these results is:

$$\frac{da}{dN} = 1 \times 10^{-11} \Delta K^3 \text{ metre/cycle } (\Delta K \text{ in MPa}\sqrt{m})$$

There is a small but perceptible frequency effect in the results shown in Figure 3 which appears to saturate with decreasing frequency, the highest propagation rates for any given value of ΔK being observed at

0.1 Hz. This could be due to a slight tendency to cyclic strain ageing although one specific study of this phenomenon in Sweden failed to find any evidence of strain ageing during fatigue crack growth[6].

3.2 De-oxgenated aqueous environments at 288°C

In this series of experiments we have examined the effect of various chemical additives used in PWR primary circuit water on corrosion fatigue crack propagation in A533-B steel. The specimens all with L-S orientation, 25 or 50 mm thick, were manufactured from either cast C8938 or 63758.1 (Table 2). The results for one cyclic frequency of 0.0167 Hz (chosen to imitate the conditions under which considerably enhanced rates of crack growth had been observed elsewhere[2,7]) are shown in Figure 4.

The most important observation is that the chemical additives, boric acid, lithium hydroxide and molecular hydrogen in the concentration ranges encountered in PWR primary circuits have only relatively little influence on fatigue crack growth rates when compared with the inert helium environment for a frequency of 0.0167 Hz and R ratios in the range 0.2 to 0.7. Secondly, throughout this work, we have been unable to sustain crack propagation at 0.0167 Hz for values of ΔK less than 15 MPa $\sqrt{m}$, whereas at higher cyclic frequencies (1.0 Hz say) or in an inert environment, no such difficulty was encountered. There is strong evidence from experiments where the crack has been extended and the crack tip sharpened by a burst of high frequency cycles followed by a return to 0.0167 Hz that this arrest phenomenon is due to oxide films forming on the crack flanks and at the tip, i.e. passivation. We also describe in the next section how raising the oxygen concentration can cause an arrested crack to start propagating again.

At relatively high values of ΔK, the evidence in Figure 3 shows that the slope of the crack growth curve decreases and approaches a value of two. Such behaviour is well known in tough, ductile steels in inert environments and considerable benefit would arise in crack propagation calculations on reactor pressure vessels by taking account of this fact[5]. Nevertheless, a safe, single, upper bound

equation to these results is:

$$\frac{da}{dN} = 4 \times 10^{-11} \cdot \Delta K^3 \text{ metres/cycle } (\Delta K \text{ in MPa } \sqrt{m})$$

Clearly, the lack of an appreciable environmental effect on crack growth at a cyclic frequency of 0.0167 Hz is in apparent conflict with results from other laboratories (see Fig. 9[2,7]) and the reasons for this are discussed in a later section.

Another series of tests using de-oxygenated aqueous environments were carried out in which the influence of specimen orientation was briefly examined. The specimens with either L-S or S-T orientation were manufactured from casts C8938 and C8982 respectively (see Table 2). Unfortunately this introduces some ambiguity into the significance of orientation to be drawn from the results, but the chemical compositions of the casts were very similar. The results are shown in Figure 5 for two frequencies of 1.0 Hz and 0.0167 Hz and a single R ratio of 0.7.

There is a uniform difference in the crack growth results at each test condition which is thought to be primarily due to orientation; the S-T orientation being particularly poor because the crack plane is in the plane of any non-metallic inclusions arising from the plate rolling process. The results in Figure 5 also show that temperature influences crack growth rates, those at 288°C being about double those measured at 20°C. Another interesting feature of the results is a small plateau-like feature in crack growth rates between 1.5 and 2.5 x 10^{-7} metres/cycles for a high frequency, 1.0 Hz, in pure water or water plus lithium hydroxide. This is particularly significant for the mechanistic model developed later.

A third series of tests in PWR primary water was initiated with specific intention of testing this mechanistic model of the origin of the very severe enhancement of crack growth rates observed in other laboratories at low cyclic frequencies and high R ratios. However, in this case, high cyclic frequencies have been used in the range 1 to 5 Hz in combination with very high R ratios of 0.7 to 0.8. The results for 50 mm or 25 mm thick L-S orientation specimens manufactured from

cast C8938 and 63758.1 respectively (Table 2) are given in Figure 6 and quite clearly show the plateau feature in crack growth rates; i.e. constant crack growth rate independent, over a specific range, of ΔK. Further experiments in this series are still in progress.

3.3 Oxygenated aqueous environments at 288°c

It is known that very small concentrations of oxygen in high temperature water can have a very profound influence on the electrochemical potential of ferritic steels[8] and by implication on corrosion and possibly corrosion fatigue kinetics. It could also be anticipated that under such conditions, contact with more noble materials (at 288°C) and the flowrate conditions would also be important; the latter because the width of a laminar flow boundary layer could result in diffusion controlled oxidation kinetics rather than by the bulk solution oxygen concentration. Thus, the effect of oxygen, whether present as an intentional additive as in BWR water simulations or unintentionally in other experiments, was an important parameter to investigate.

In our experience, controlling precise low levels of oxygen in solution has been difficult, requiring precise metering of the oxygenated water flow and a knowledge of the oxygen consumption characteristics of the water loop pipework. We conclude that inadvertent oxygen contamination other than as an initial experimental transient is unlikely except where there is a continuous uninterrupted supply, for example, though a leaking pump gland.

The experimental results for the influence of oxygen at various concentrations on corrosion fatigue crack propagation in 25 or 50 mm specimens with L-S orientation, manufactured from casts C8938 or 63758.1 respectively (Table 2), are shown in Figure 7. The sine wave cyclic frequency was 0.0167 Hz and the R ratio was varied between 0.2 and 0.7. No effect of steel cast was observed but an influence of oxygen concentration on crack propagation rates is evident in Figure 7 for concentrations in excess of 100 ppb up to 500 ppb. In these cases, high rates of crack growth were observed initially in each experiment comparable with the worst observed by others in either simulated normal

BWR water (200 ppb oxygen[9,10]) or simulated PWR primary water (< 10 ppb oxygen[2,7]). However, these high rates of growth were only measured for the first few millimetres of crack growth following in situ pre-cracking at a relatively high frequency of 1.0 Hz. The rate of crack growth decelerated over the first few days of each experiment, after which the cracks grew as though the oxygenated water were not present. An experiment was also carried out in which the crack growth rate was allowed to decay in the manner just described, followed by a burst of high frequency cycles (1.0 Hz) at the same cyclic stress in order to push the fatigue crack on a few millimetres over a period of a few hours. After this procedure the cyclic frequency was reduced to 0.0167 Hz and the high initial rate of crack growth was restored, which then decayed away as before. In another experiment a fatigue crack propagating at 1.0 Hz at ΔK = 15 MPa$\sqrt{m}$ in deoxygenated pure water was allowed to arrest by reducing the frequency to 0.0167 Hz at the same cyclic stress, and then oxygen was injected at a concentration of 1200 ppb. The outlet oxygen concentration (probably most representative of the bulk loop concentration) rose steadily over a period of a few days and when it reached 1100 ppb, the crack suddenly started propagating again, but not at an unusually fast rate.

All these observations, and particularly the last one mentioned above, are not consistent with a crack blunting mechanism as either the reason for the decay in crack growth rate observed in oxygenated water or the arrest of cracks at low cyclic frequencies for ΔK = 15 MPa$\sqrt{m}$ in de-oxygenated water. Only a passivation mechanism is capable of explaining all the features of these observations. Thus oxide films on the specimen and particularly the crack flanks reduces the dissolution rate which can be sustained at the crack tip and, apparently, can block fatigue slip step emergence at the crack tip at low values of ΔK. Oxygen, at the concentrations used, enhances dissolution but is always eventually negated by the passivation process. The quantitative implications of this description are addressed in the Discussion section.

The influence of the applied cyclic frequency has also been examined in a short series of experiments using simulated BWR water (i.e. 100-200 ppb) and a single stress ratio, R = 0.7. The results are

shown in Figure 8. At cyclic frequencies between 0.1 and 1.0 Hz a small pateau feature around 1 to 2 x 10^{-7} metres/cycle was observed unlike the results for the low frequency of 0.0167 Hz, where the initial high crack growth rates decayed to the normal inert environment rate as described above. These plateaux in crack growth are considered to be significant, particularly as it is now known that at very high oxygen concentrations of ~ 1200 ppb the high crack growth rates, which we observed only in the initial stages of our experiments with lower oxygen concentrations, can be sustained at very low cyclic frequencies (see Fig. 10[11,12]).

4. DISCUSSION

It is clear from the results described above that there is a major discrepancy between the experimental data reported here for PWR primary water environments and those described by Bamford et al[2,7] reproduced here in Figure 9. It has been suggested that the sulphur content of the steel may be a factor[13], in that all the results described in this paper refer to modern, relatively clean steels, while those in Figure 9 refer mainly to older, dirtier steels. We believe that steel sulphur content may indeed play an important role but that this can only be clearly understood if metallurgical factors such as this one and water chemistry variables are considered together. Both sets of variables will combine under some circumstances to produce adverse electrochemical conditions while other combinations are benign. Measurements of electrochemical potential are therefore seen as an important requirement to improve our understanding of the basic processes in any future work.

The importance of passivation kinetics in accounting for the influence of oxygen has been cited earlier. An independent examination of the oxide films on the steel specimens in this programme exposed to water or water + LiOH at 288°C has revealed important differences in morphology and oxide tenacity from those produced by Bamford et al under nominally the same conditions[14]. This is important prima facie evidence that the electrochemical conditions within the two experimental rigs are different. One obvious physical difference is the flowrate regime each experimental rig operates in; the one

described here having a much faster flowrate and almost certainly turbulent flow over the specimen. Moreover, in an international 'round robin' series of tests described in another paper at this conference[15] the plateaux features in the crack propagation curve were seen in static or low flow autoclaves but not in the high flowrate conditions used in this work. It is these plateaux rates of crack growth which appear to be the main difference between those results which show very large enhancements in crack growth rates compared to an inert environment and those which do not. It is suggested that this plateau phenomenon is in reality due to stress corrosion cracking, where chemical reaction rates rather than the applied ΔK control the rate of crack advance, and that the electrochemical conditions which allow this to occur or not is the crucial difference between individual laboratories.

Stress corrosion cracking tests of the classical type, where pre-cracked, bolt loaded, compact tension specimens of A533-B, A508-II and weldments thereof have been used, have been in progress in simulated (low flowrate) PWR water for several years[13]. In all tests on plate steel, forging steel or weld metal, no crack extension has occurred even after 40,000 hours. However, in the case of the weld HAZ specimens, crack growth has occurred in every case within 2000 hours at stress intensities as low as 48 MPa $\sqrt{m}$. This evidence, as it stands, does not immediately suggest that stress corrosion cracking would be a problem in corrosion fatigue tests on any materials other than weld HAZs.

It is, however, well known that applied cyclic stresses of relatively small amplitude can depress the apparent static load threshold for stress corrosion by about a factor of two in several ductile metal/environment combinations known to exhibit stress corrosion cracking[16]. It has been established that in such circumstances the crack initiates at some specific strain, well below the nominal static threshold, usually by rupture of a passive film, but if the dynamic strain is also not above a certain threshold value, then repassivation dominates and crack growth arrests. The sensitivity of many stress corrosion systems which depend on passive film breakdown to the applied strain rate is very well established and casts a great

deal of doubt on the value of a single static stress or stress intensity threshold parameter such as K_{Iscc}. For dynamic strain conditions, the apparent K_{Iscc} is just one necessary, but not sufficient, condition which must be satisfied for crack growth to occur, even when the electrochemical conditions for stress corrosion cracking are favourable. Application of a monotonic or cyclic stress allows a low creep rate to persist, and increases the rate of slip step emergence at the crack tip so that dissolution rates remain high and crack propagation proceeds. The work hardening properties of the metal would also be expected to be important here. Therefore, the necessary and sufficient conditions for stress corrosion cracks to start and then continue propagating are: (i) a critical crack tip strain must be exceeded (characterised by K_{Iscc} but determined dynamically), (ii) a critical crack tip strain rate, $\dot{\varepsilon}$, must also be exceeded and (iii) the electrochemical conditions must be favourable.

For a quantitative interpretation of the corrosion fatigue crack propagation kinetics, it is necessary first to estimate the crack tip strain rate during the tensile part of the fatigue cycle. In the case of small scale yielding, the crack tip opening displacement, δ, as a function of the crack tip stress intensity, K, is given by:

$$\delta \propto \frac{K^2}{E\sigma_y}$$

where E is the elastic modulus and σ_y the yield stress. The crack tip strain rate, $\dot{\varepsilon}$, is defined by:

$$\dot{\varepsilon} = \frac{1}{\delta}\frac{d\delta}{dt}$$

For sine wave cycles, where the increasing tensile strain takes place over T seconds, the stress intensity as a function of time is:

$$K = \frac{\Delta K}{2}\left[\frac{1+R}{1-R} + \cos \pi\left(1 + \frac{x}{T}\right)\right]$$

where x/t is the fraction of T seconds elapsed in the tensile half cycle. Thus, the instantaneous strain rate at any point in the cycle is:

$$\dot{\varepsilon} = \frac{1}{\varepsilon}\frac{d\varepsilon}{dx} = \frac{-2}{T}\left[\sin\left(1 + \frac{x}{T}\right)\right] \Big/ \left[\frac{1+R}{1-R} + \cos\pi\left(1 + \frac{x}{T}\right)\right]$$

Similarly for linear ramps, where the increasing strain takes place over T seconds:

$$K = \frac{\Delta K}{2}\left[\frac{1+R}{1-R} + \left(\frac{2x}{T} - 1\right)\right]$$

and

$$\dot{\varepsilon} = \frac{1}{\varepsilon}\frac{d\varepsilon}{dx} = \frac{2}{T} \cdot \frac{1}{\frac{R}{1-R} + \frac{x}{T}}$$

These functions for $\dot{\varepsilon}$ are plotted in Figure 11 as a function of x/T, from which it can be seen that $\dot{\varepsilon}$ varies in a complex way during a fatigue stress cycle. However, high R ratio cycles with ramp loading produce the most uniform crack tip strain rate during the cycle. An average measure of the tensile crack tip strain rate in a fatigue cycle is given by:

$$\dot{\varepsilon}_{av} = \frac{1}{T}\int_{\varepsilon_{min}}^{\varepsilon_{max}} \frac{1}{\varepsilon}\, d\varepsilon = \frac{2}{T} \ln \frac{1}{R}$$

This equation together with the maximum and minimum excursions in $\dot{\varepsilon}$ during a fatigue cycle are shown as a function of R ratio in Figure 12. It can be seen that to establish a correlation between the rates of crack growth and the crack tip strain rate involves a compromise if $\dot{\varepsilon}_{av}$ is used, but this is a better approximation the higher the R ratio.

In Table 3 the plateaux rates of crack growth derived from Figures 6, 9 and 10 are given as a function of $\dot{\varepsilon}_{av}$ and are plotted in graphical form in Figure 13. Data for cycles with hold times at constant stress have been excluded. These rates of crack growth have been converted to a time base and corrected, where necessary, for the component of fatigue crack growth which would occur anyway in an inert

environment. In the case of relatively low R ratios in particular, a correction was also made for the fraction of the cycle spent with K above the stress corrosion threshold, i.e. the apparent dynamic K_{Iscc}. A value of 28 MPa $\sqrt{m}$ appears to fit the threshold data quite well. Table 4 shows values of ΔK as a function of R for which K_{max} or K_{min} exceed 28 MPa $\sqrt{m}$. It can be seen from Figure 13 that a correlation exists between $(da/dt)_{plateau}$ and $\dot{\varepsilon}_{av}$.

Independent measurements of dissolution transients have been made for two different stainless steels following sudden increases in strain in water (plus sodium sulphate to confer electrical conductivity) at 97°C[17]. These transients, i, decay over periods of tens of seconds as:

$$i = i_o (t - t_o)^{-\frac{1}{2}}$$

although for the first few milliseconds the decay rate is exponential. On the basis of these observations and a low measured activation energy of $\sim$4 Kcal/mole, a kinetic model was derived based on crack tip cation solvation and transport as the rate determining processes[17]. Thus if the same rate determining processes were relevant to the plateaux rates of crack growth, during corrosion fatigue at low frequencies, then da/dt should be a function of $\dot{\varepsilon}^{\frac{1}{2}}$ as indeed appears to be the case in Figure 13. The upper bound drawn on the graph obeys the equation:

$$\frac{da}{dt} = 5 \times 10^{-4} \dot{\varepsilon}_{av}^{\frac{1}{2}} \quad \text{mm/sec}$$

It seems likely that cycles with hold times at constant stress will give, effectively, rather lower plateau rates than cycles without such periods.

Another deduction can be made from the electrochemical dissolution transient measurements[17], concerning the maximum possible bare surface dissolution rates and hence the maximum possible rate of electrochemical crack penetration. The maximum current densities measured at 97°C were 2 and 0.25 amps/cm^2 for potentials of +100 and -400 mv (wrt S.C.E.) respectively. From Faraday's law of electrochemical equivalents:

$$\left(\frac{da}{dt}\right)_{max} = \frac{i_{max} M}{ZF \rho}$$

where Z is the number of electrons involved in the reaction, ρ is the density, M is the molecular weight and F = 96,500 coulombs/equivalent is the Faraday. These maximum possible penetration rates are plotted on Figure 13 and agree within an order of magnitude with the plateaux rate observed in the corrosion fatigue experimental results deduced from Figure 6. The activation energy to convert these calculated maximum penetration rates from 97°C to 288°C is at present not known. It is apparent that in these fairly high frequency experiments, the oxide rupture rate exceeded the rehealing or repassivation rate.

From Figure 13 it is possible to deduce that in our experiments with A533-B steel in PWR water, strain rate sensitive stress corrosion is possible for strain rates greater than 1 sec^{-1}. For the low oxygen concentration, BWR environment data in Figure 8, the plateau rates of crack growth are observed at values of $\dot{\varepsilon}$ as low as 0.14 sec^{-1}. It is probable that a lower strain rate threshold is appropriate to that environment. In water at 288°C containing 8000 ppm oxygen, there is enough evidence to suggest that the threshold strain rate is in the region of 10^{-8} sec^{-1} (17,18). This is consistent with well established notions for other stress corrosion systems that the threshold strain rate depends on the electrochemical potential(16). Figure 13 can therefore be divided into three zones; a zone where bare surface dissolution rates are controlling, a zone where diffusion processes within the fluid are rate controlling and a threshold value of $\dot{\varepsilon}$ which depends on the water chemistry, and, very probably, on the steel metallurgy; in other words, the electrochemical potential. It is clear that the threshold for the electrochemical conditions with PWR water in our experimental rig is between 0.1 and 1 sec^{-1} and in fact probably close to the larger of these two values. From the results of Bamford et al, it is suggested that the threshold for the stress corrosion phenomenon is around 0.01 sec^{-1} since high corrosion fatigue crack propagation rates were not observed in experiments at 0.1 cpm and R = 0.2. In fact the

rates of crack propagation in these particular tests were close to the inert environment fatigue crack growth rates, despite the fact that the value of K exceeded the threshold of 28 MPa$\sqrt{m}$.

It is possible from the above treatment of the corrosion fatigue results in terms of a fatigue plus strain rate sensitive stress corrosion mechanism to derive a map of combinations of R ratios and cyclic frequencies where the resulting strain rate will give resolvable plateau features in corrosion fatigue experiments. Such a map is shown in Figure 14 which divides into four basic areas; (i) where the fatigue crack growth rate is always faster with respect to time than the bare surface dissolution penetration rate, (ii) where the bare surface dissolution kinetics controls the plateau rate, (iii) where diffusion kinetics control the plateau rate and (iv) where passivation prevents stress corrosion cracking and either the crack arrests completely or only grows at the appropriate fatigue crack growth rate. Such a diagram was used in combination with Figure 13 to plan the experiments which led to the experimental results shown here in Figure 6.

Finally a calculation scheme for predictive purposes can be derived on the basis of the model using the principle of superposition of fatigue crack growth and stress corrosion cracking. The equation is:

$$\frac{da}{dN} = C_1 \Delta K^n + TC_2 \left(\frac{2}{T} \ln \frac{1}{R}\right)^{\frac{1}{2}} \left(1 - \frac{x}{T}\right)$$

where C_1, C_2 and n are constants, T is the tensile going period of any fatigue stress and $(1 - \frac{x}{T})$ takes values between zero and one for K_{min} ' K_{Iscc} ' K_{max}. Some examples are shown on a standard fatigue crack growth graph in Figure 15.

5. CONCLUSIONS

(i) Fatigue crack propagation rates have been determined for A533-B steel in an inert helium environment at 288°C, the upper bound being

$$\frac{da}{dN} = 1 \times 10^{-11} \Delta K^3 \text{ metres/cycle } (\Delta K \text{ in MPa}\sqrt{m})$$

This crack growth equation predicts faster crack propagation rates than the current ASME XI Appendix A code for dry cracks when $\Delta K < 50$ MPa $\sqrt{m}$, but slower rates for $\Delta K > 50$ MPa$\sqrt{m}$.

(ii) Corrosion fatigue crack growth data for a modern heat of A533-B steel in a PWR primary water environment have been determined at 0.0167 Hz (1 cycle/minute) for R ratios of 0.2, 0.5 and 0.7. The upper bound to these data is:

$$\frac{da}{dN} = 4 \times 10^{-11} \Delta K^3 \text{ metres/cycle } (\Delta K \text{ in MPa}\sqrt{m})$$

The high crack growth rates observed in nominally the same experiments in the USA[2,7] have not been reproduced.

(iii) Corrosion fatigue crack growth data for A533-B steel in simulated BWR environments containing 100 to 500 ppb oxygen have shown a marked but transitory effect of oxygen on crack growth rates. Passivation causes these transient high growth rates to decay and eventually rates of growth appropriate to deoxygenated environments are observed.

(iv) A mechanistic model to explain these observations and those of other investigators who have observed much higher sustained crack propagation rates in either low flowrate simulated PWR water or air saturated BWR water has been described. It is suggested that the observation of unusually high corrosion fatigue crack growth rates is dependent on the coincident operation of a strain rate sensitive stress corrosion process. Whether this phenomenon is observed or not depends primarily on the electrochemical potential, itself a result of a combination of metallurgical and water chemistry factors and, conceivably, electrical coupling with dissimilar materials.

(v) A quantitative calculation scheme based on conclusion (iv) has also been developed and has been used to define the experimental conditions required to observe chemical reaction rate dominated crack growth processes during corrosion fatigue tests. Experiments defined with the help of the model have been carried out and the evidence obtained supports the quantitative predictions within the range of variables tested so far.

References

1. T. Kondo, T. Kikuyama, H. Nakajima, M. Chindo and R. Nagasaki, Proceedings of a Conference on "Corrosion Fatigue: Chemistry, Mechanics and Microstructure", p. 539-556, University of Connecticut, USA, 14-16 June 1971.

2. T.R. Mager, D.M. Moon and J.D. Landes, Transactions of the ASME, J. of Pressure Vessel Technology 99 (1977), 238-247.

3. P.M. Scott and A.E. Truswell in "The measurement of crack length and shape during fracture and fatigue", p. 69-84, Engineering Materials Advisory Services Ltd., 1980.

4. ASME Section XI (1980).

5. P.M. Scott and B. Tomkins, IAEA Specialists Meeting on Corrosion Fatigue, Freiburg, 13-15 May 1981.

6. J. Wiberg, Int. J. Press Ves. & Piping, 8 (1980) 79-90.

7. W.H. Bamford, Transactions of the ASME, J. of Engineering Materials and Technology 101 (1979) p. 182-190.

8. M.E. Indig, Report NEDC 24625 (1979).

9. D.A. Hale, C.W. Jewett and J.N. Kass, Transactions of the ASME, J. of Engineering Materials and Technology 101 (1979) p. 191-198.

10. D.A. Hale, J. Yuen and T. Gerber, Report GEAP-24098 (1979) and D.A. Hale, Report NEDC 25322 (July 1980).

11. T.A. Prater and L.F. Coffin, Report NEDC 25322 (July 1980).

12. T. Williams, Private communication.

13. W.H. Cullen, F.J. Loss, H.E. Watson, W.H. Bamford and L.J. Ceschini, "Influence of critical variables on environmentally-assisted crack growth rates of RPV materials in PWR coolant environments", 8th Water Reactor Safety Information Meeting, Gaithersburg, Maryland, USA, October 1980.

14. A. McMinn, Private communication.

15. R. Jones, IAEA Specialists Meeting on Corrosion Fatigue, Freiburg 13-15 May 1981.

16. R.N. Parkins, Conference on "Defects and crack initiation in environment sensitive fracture", Newcastle University, 12-14 Jan 1981. To be published in Metal Science.

17. F.P. Ford and M. Silverman, Report HTGE 451-8-12 (1979).

18. F.P. Ford and M.J. Povich, G.E. Report No. 79 CRD 007 (1979).

Table 1

PWR and PWR Water Chemistry Specification

	BWR		PWR	
	Specification	Typical in this work	Specification	Typical in this work
Pressure, MPa	6.9	8.0 ± 0.2	17.2	15.0 ± 0.5
Temperature, °C	288	288 ± 0.5	288-315	288 ± 0.5
Conductivity, (inlet), $\mu S\ cm^{-1}$	< 0.1	< 0.08	1-40	25 ± 2
Conductivity (outlet), $\mu S\ cm^{-1}$		< 1.0		25 ± 2
Oyxgen, ppb	50-200	< 10-1000 as required For > 200 ± 100	100	10
Hydrogen, ml/kg at STP	-	-	0-50	40
LiOH, ppm	-	-	0.6-6.2	2.4-6.2
H_3BO_3, ppm	-	-	0-13000	10000-13000
Cl^-, ppm	< 0.1	0.06	< 0.15	0.06
F^-, ppm	< 0.1	< 0.02	< 0.15	< 0.02
pH (room temperature)	6.5-7.0	6.5-7.0	4.0-10.5	5.6 ± 0.1

Table 2

Composition (%) and Mechanical Properties at 20°C
of SA 533 Grade B Class 1 Steel

	ASME specification	S-T orientation specimens	L-S orientation specimens	T-L orientation specimens	L-S orientation specimens
Cast		C8982	C8938	1bH	63758.1
Country of Origin		UK	UK	USA	France
Carbon	0.25 (max)	0.19	0.21	0.19	0.185
Manganese	1.01-1.66	1.25	1.24	1.28	1.395
Phosphorus	0.035 (max)	0.017	0.016	0.009	0.010
Sulphur	0.040 (max)	0.013	0.012	0.013	0.006
Silicon	0.13-0.32	0.025	0.20	0.25	0.195
Molybdenum	0.41-0.64	0.49	0.49	0.55	0.485
Nickel	0.37-0.73	0.68	0.66	0.61	0.655
Chromium	-	0.13	0.08	0.04	0.130
Vanadium	-	-	-	0.004	-
Copper	-	0.07	0.09	0.10	0.095
Aluminium	-	-	-	-	0.022
Cobalt	-	0.009	0.013	-	-
Tin	-	0.011	0.012	-	-
Tantalum	-	0.002	0.002	-	-
Tensile strength MPa	552-689	579-585	571-601		607-612
Yield strength (0.2% offset) MPa	344	395-435	398-408	386	468-472
Elongation in 50 mm %	18	29	23-35		28-29
Reduction in area %	-	66	62		-

Table 3

'Plateau' Rates of Corrosion Fatigue Crack Growth

Reference	$(\frac{da}{dN})_{obs}$ mm/cycle	ΔK MPa$\sqrt{m}$	R	f Hz	T secs	$1-\frac{x}{T}$ for K > 28 MPa$\sqrt{m}$	$(\frac{da}{dN})_{scc}$ mm/cycle	$(\frac{da}{dt})_{scc}$ mm/sec	$\dot{\varepsilon}$ sec^{-1}
Water + 8.0 ppm	2.9×10^{-2}	20 to 24	0.5	0.00021	4230	0.6 to 0.8	2.9×10^{-2}	9.6×10^{-6}	3.2×10^{-4}
oxygen at 288°C	7.3×10^{-3}	22 to 30	0.5	0.0021	432	0.7 to 1.0	7.3×10^{-3}	2.0×10^{-5}	3.2×10^{-3}
A333-6 steel	1.8×10^{-3}	25 to 28	0.5	0.021	43.2	0.9 to 1.0	1.8×10^{-3}	4.6×10^{-5}	3.2×10^{-2}
Reference 11	1.0×10^{-2}	44 to 50	0.2	0.0021	432	0.6 to 0.7	1.0×10^{-2}	3.6×10^{-5}	7.5×10^{-3}
	1.5×10^{-3}	7 to 9	0.8	0.0021	432	1.0	1.5×10^{-3}	3.5×10^{-6}	1.03×10^{-3}
PWR water at 288°C	6×10^{-3}	45 to 80	0.25	0.0083	60	1.0	6×10^{-3}	1.0×10^{-4}	4.6×10^{-2}
A533-B	3×10^{-3}	35 to 100	0.16	0.0167	30	0.4 to 0.8	3×10^{-3}	1.7×10^{-4}	1.2×10^{-1}
A508-II	6×10^{-3}	20	0.70	0.0083	60				
and welds			0.70	0.0167	30				
References 2,7	1.1×10^{-3}	15 to 25	0.67	0.0167	30	1.0	1.1×10^{-3}	3.5×10^{-5}	2.7×10^{-2}
	2.3×10^{-3}	22	0.22	0.0167	30	0.7	2.3×10^{-3}	1.4×10^{-4}	1.0×10^{-1}
	3.2×10^{-3}	40 to 60	0.21	0.0167	60	0.6 to 0.8	3.2×10^{-3}	7.6×10^{-5}	5.2×10^{-2}
	2.5×10^{-3}	20 to 25	0.70	0.0167	60	1.0	2.5×10^{-3}	4.2×10^{-5}	1.2×10^{-2}
'Round Robin'	2.7×10^{-3}	45 to 60	0.2	0.0167	30	0.6 to 0.7	2.1×10^{-3}	1.1×10^{-4}	1.1×10^{-1}
Pure water at 288°C									
A533-B									
Reference 15									
This work	1.5×10^{-4}	23 to 30	0.7	1.0	0.5	1.0	1.5×10^{-4}	3.0×10^{-4}	1.43
PWR water at 288°C	2.1×10^{-5}	12 to 16	0.7	5.0	0.1	0.8 to 1.0	1.7×10^{-5}	1.7×10^{-4}	7.1
A533-B	2.5×10^{-5}	7 to 11	0.8	5.0	0.1	1.0	2.1×10^{-5}	2.1×10^{-4}	4.5

Note: f = cyclic frequency, T = that part of the cyclic period with the tensile strain increasing

$1-\frac{x}{T}$ = fraction of tensile period spent with K > 28 MPa$\sqrt{m}$.

$$(\frac{da}{dN})_{scc} = (\frac{da}{dN})_{obs} - (\frac{da}{dN})_{fatigue} \qquad (\frac{da}{dt})_{scc} = (\frac{da}{dN})_{scc} \cdot \frac{1}{T(1-\frac{x}{T})} \qquad \dot{\varepsilon} = \frac{2}{T} \ln \frac{1}{R}$$

Table 4

Values of ΔK required for K_{min} or K_{max} in a fatigue cycle to exceed a value of K_{Iscc} = 28 MPa$\sqrt{m}$ as a function of R ratio

$R = \frac{K_{min}}{K_{max}}$	K_{max} = 28		K_{min} = 28	
	ΔK	K_{min}	ΔK	K_{max}
0	28	0		
0.1	25.2	2.8	252	280
0.2	22.4	5.6	112	140
0.3	19.6	8.4	65.3	93.3
0.4	16.8	11.2	42	70
0.5	14	14	28	56
0.6	11.2	16.8	18.7	46.7
0.7	8.4	19.6	12	40
0.8	5.6	22.4	7	35
0.9	2.8	25.2	3.1	31.1
0.95	1.4	26.6	1.5	29.5

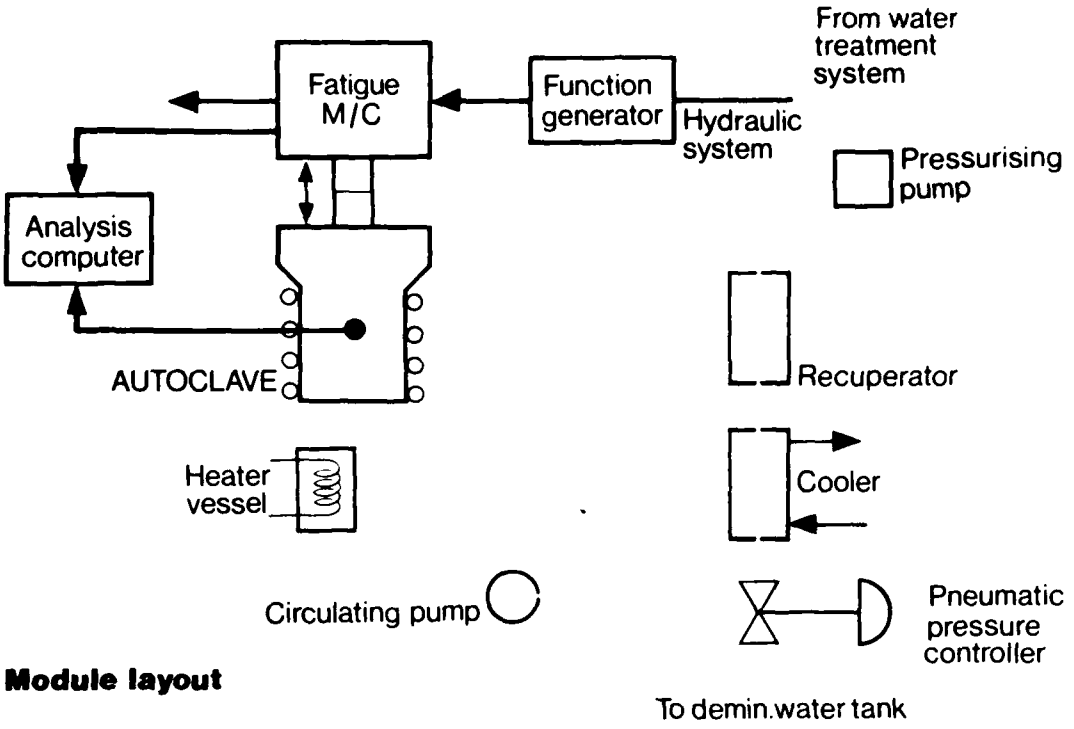

Module layout

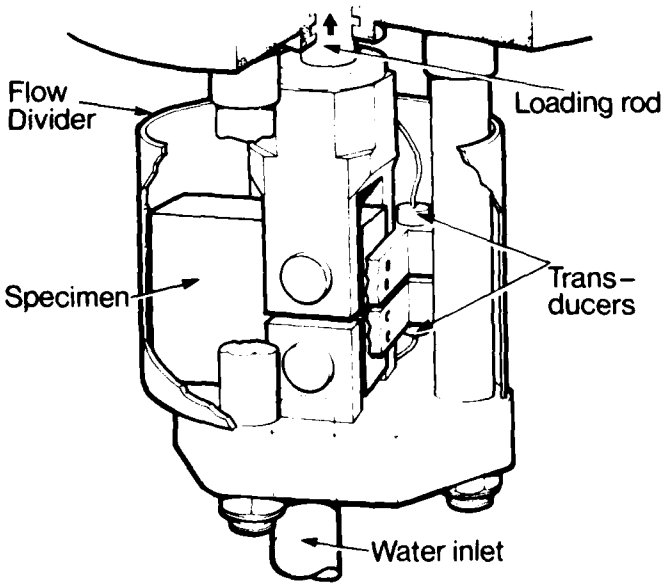

Specimen mounted in autoclave

AERE - R 10201 Fig. 1
Schematic diagrams of the Corrosion Fatigue Test Rig

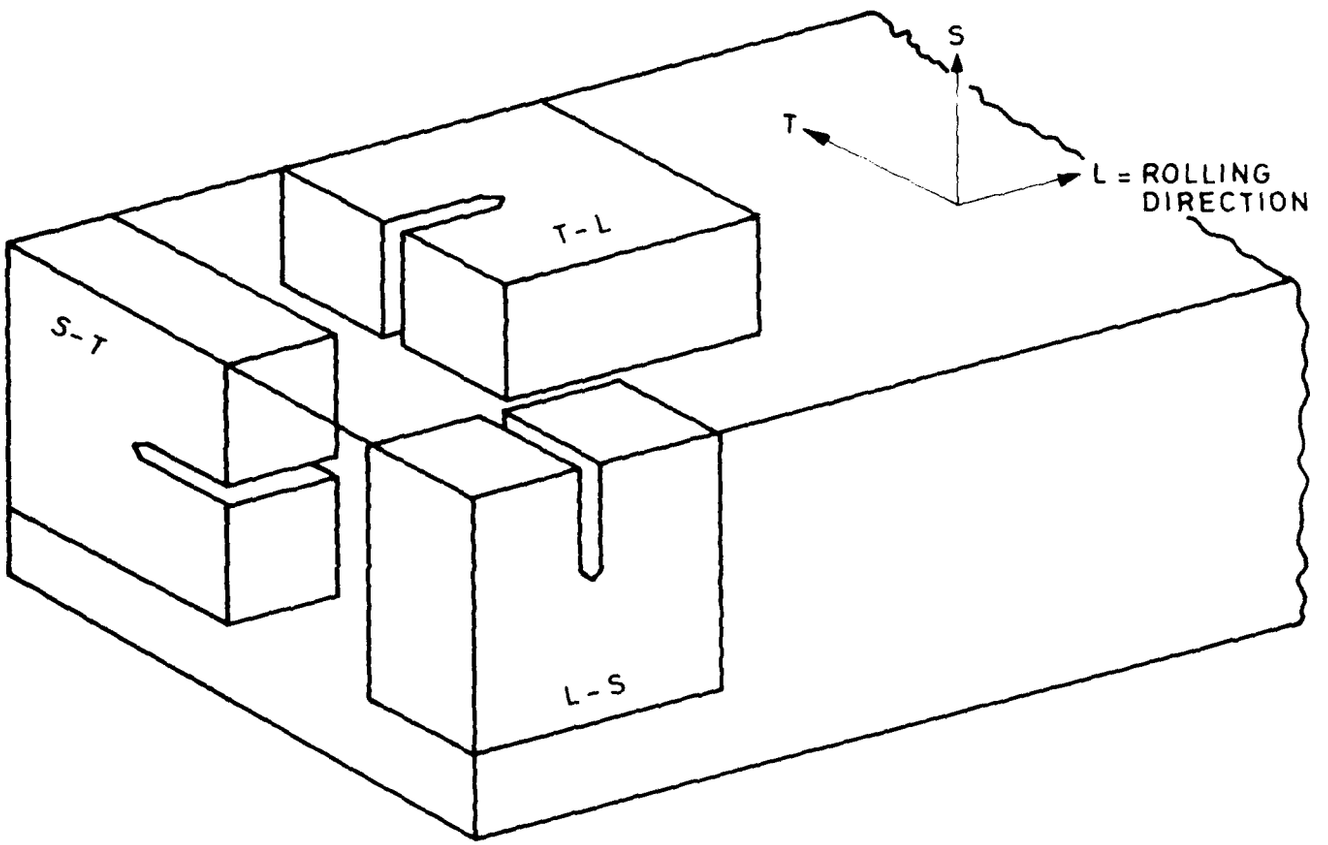

AERE - R 10201 Fig. 2
Specimen orientations

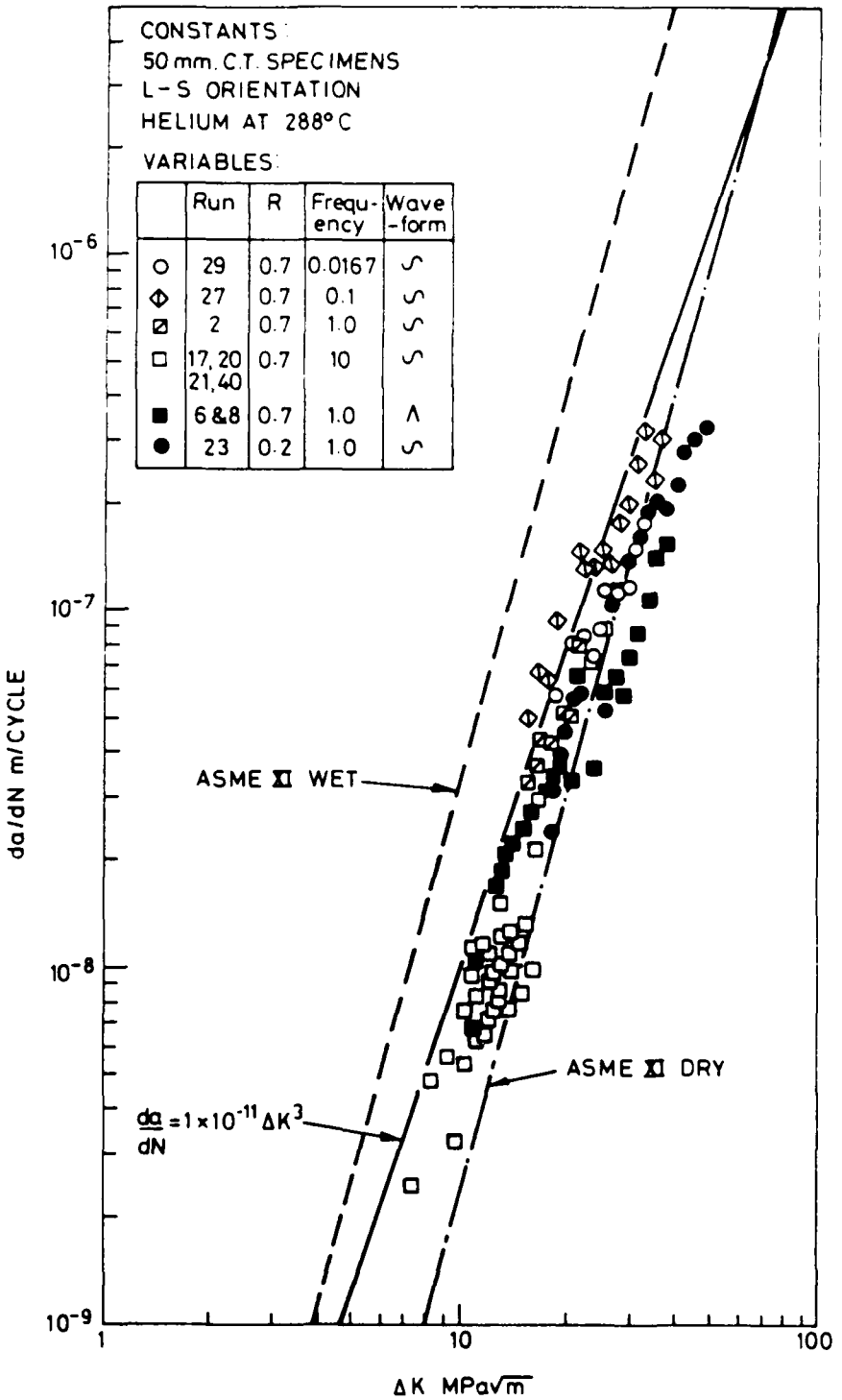

AERE - R 10201 Fig. 3
Crack propagation data for A533-B steel in helium at 288°C

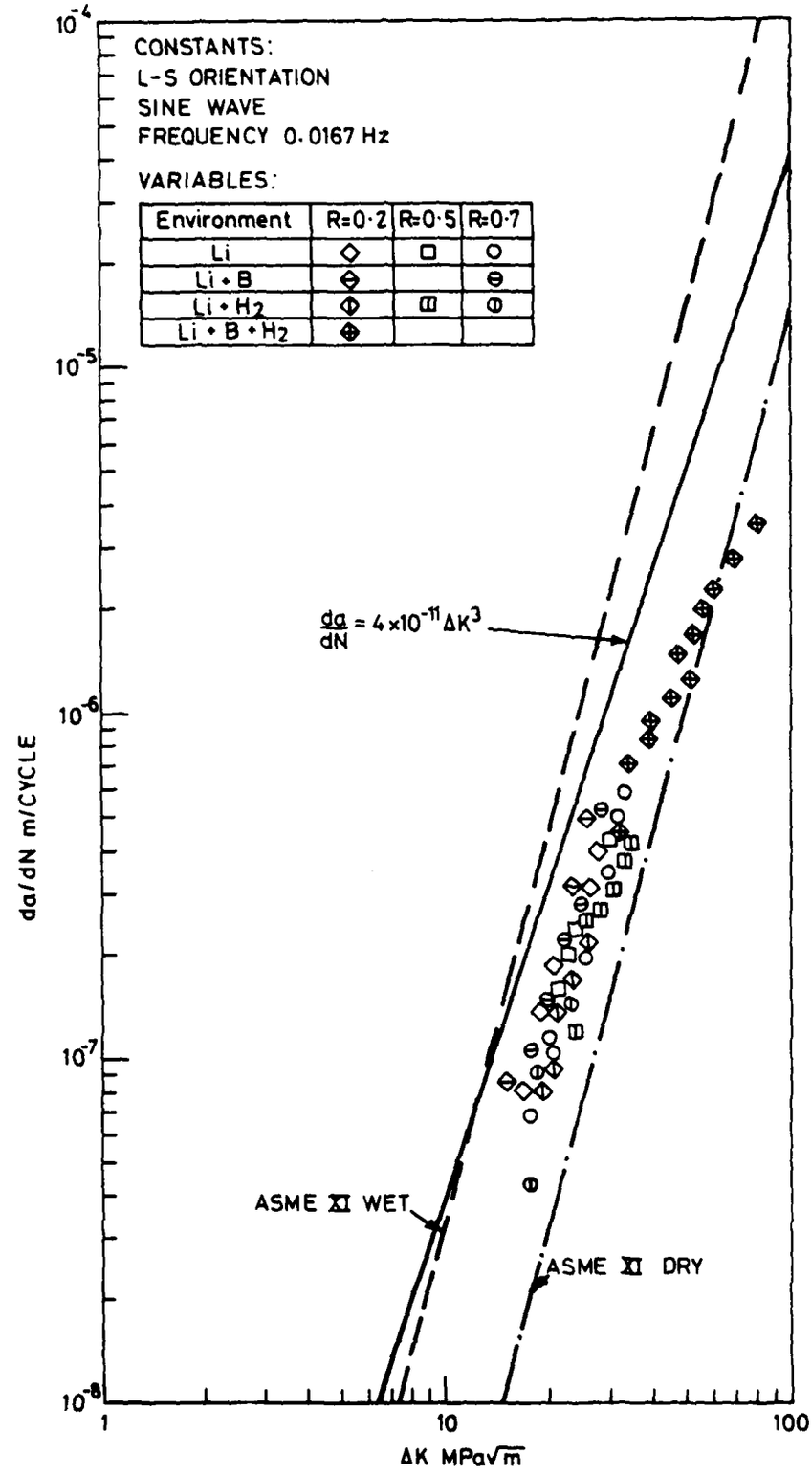

AERE - R 10201 Fig. 4

Influence of PWR water conditions on crack propagation rates in A533–B steel at 288°C

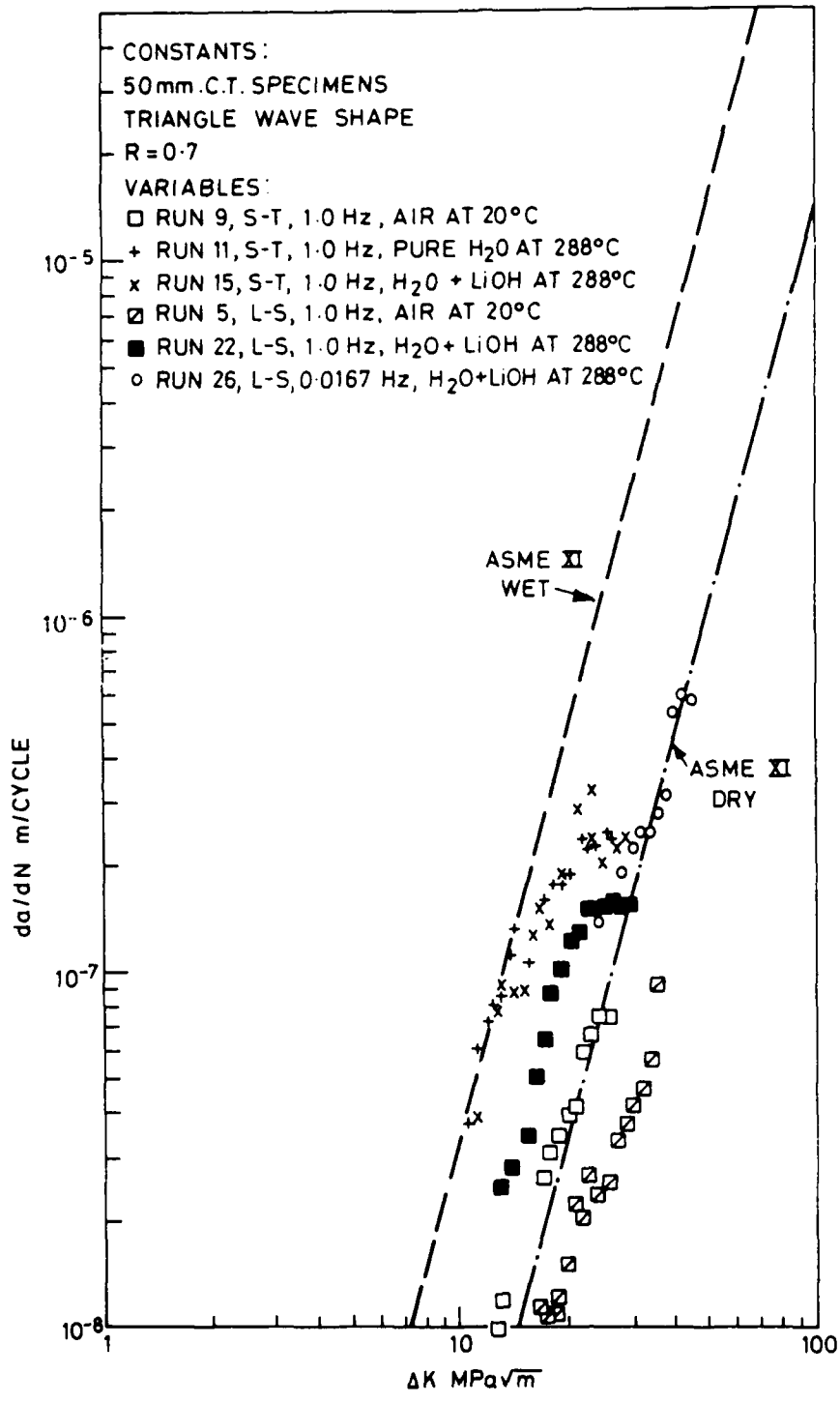

AERE - R 10201 Fig. 5
Results for S–T orientation specimens of A533–B steel and comparison with L–S orientation specimens

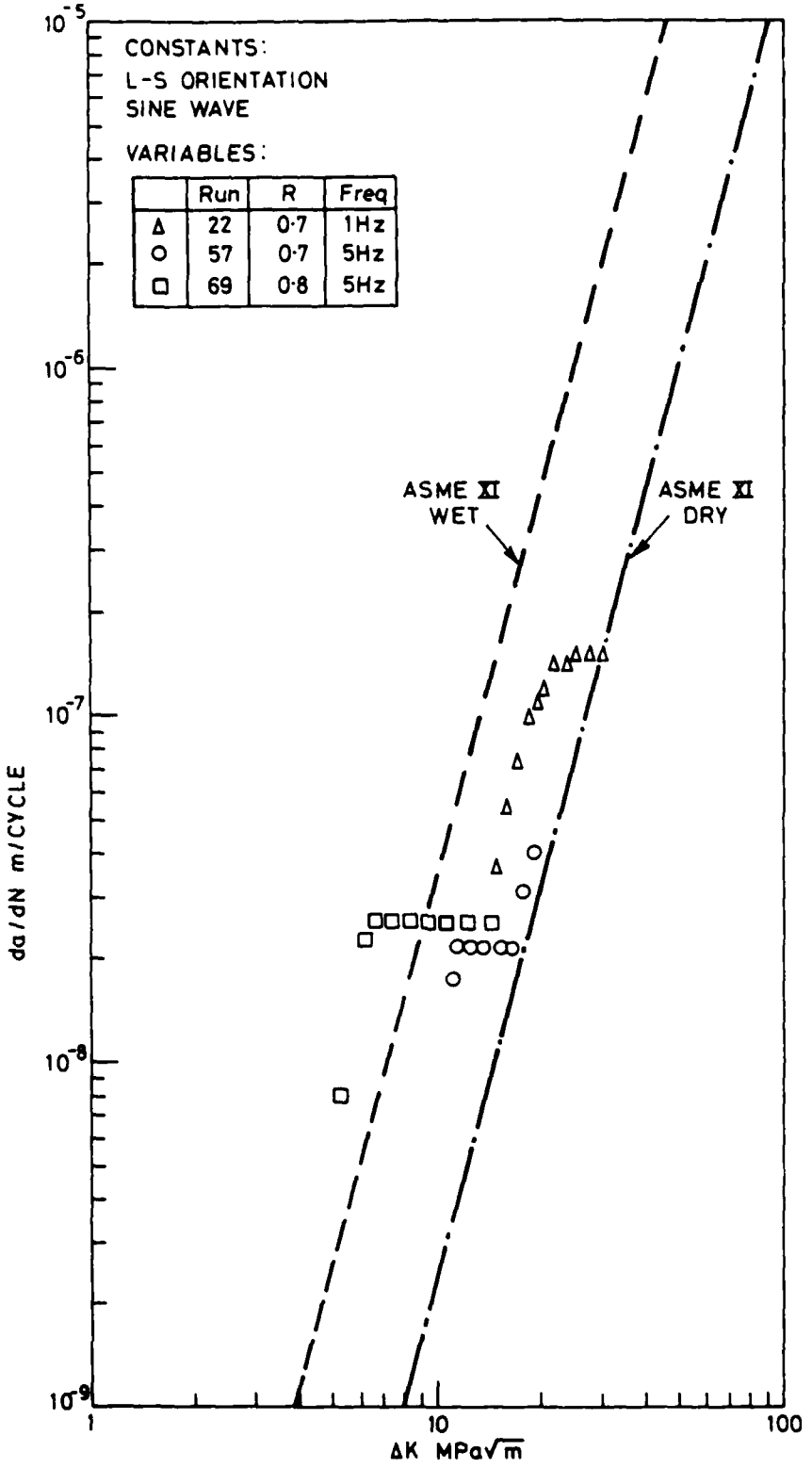

AERE - R 10201 Fig. 6

Influence of R ratio and frequency on crack propagation rates in A533–B steel in PWR water at 288°C

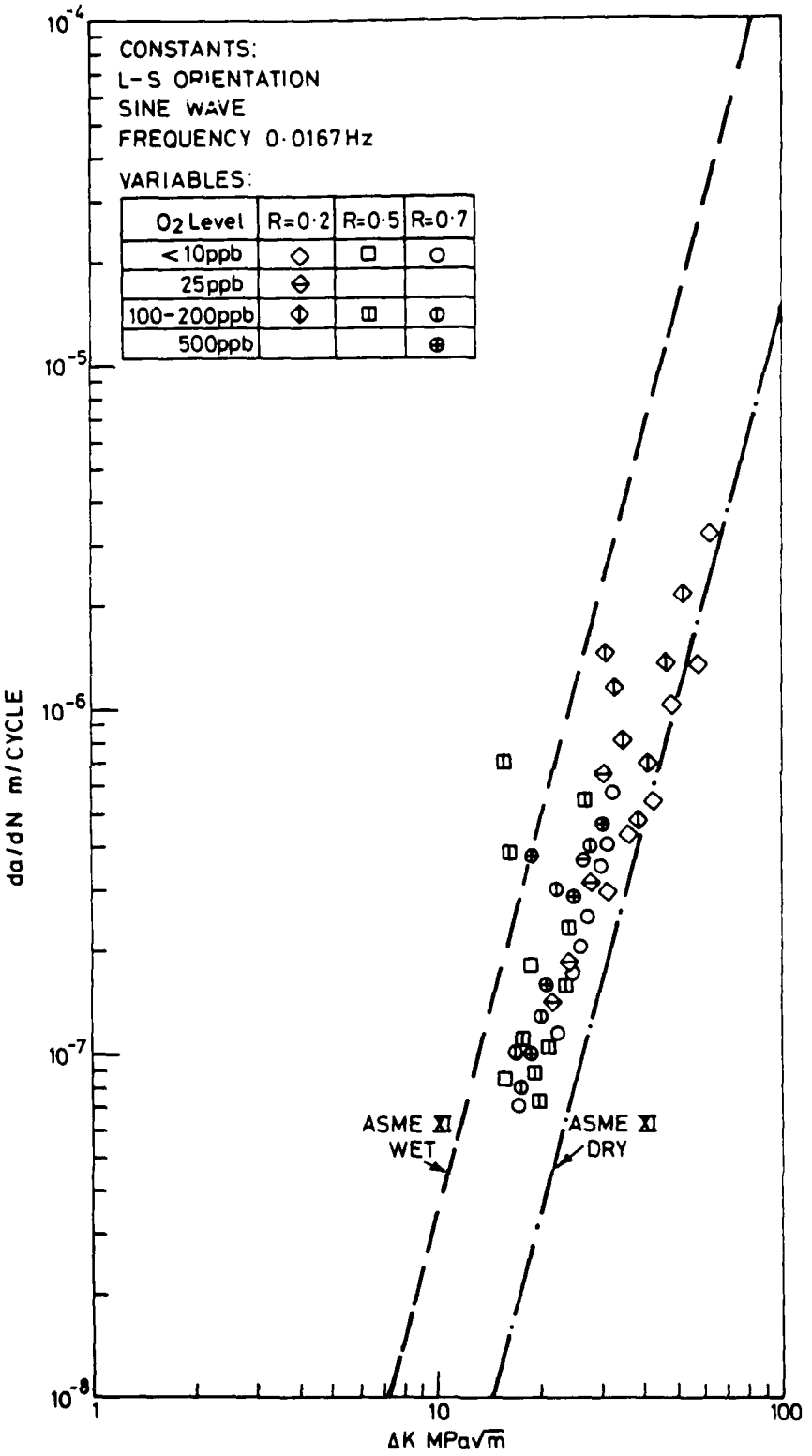

AERE - R 10201 Fig. 7

Influence of oxygen level on crack propagation rates in A533-B steel at 288°C

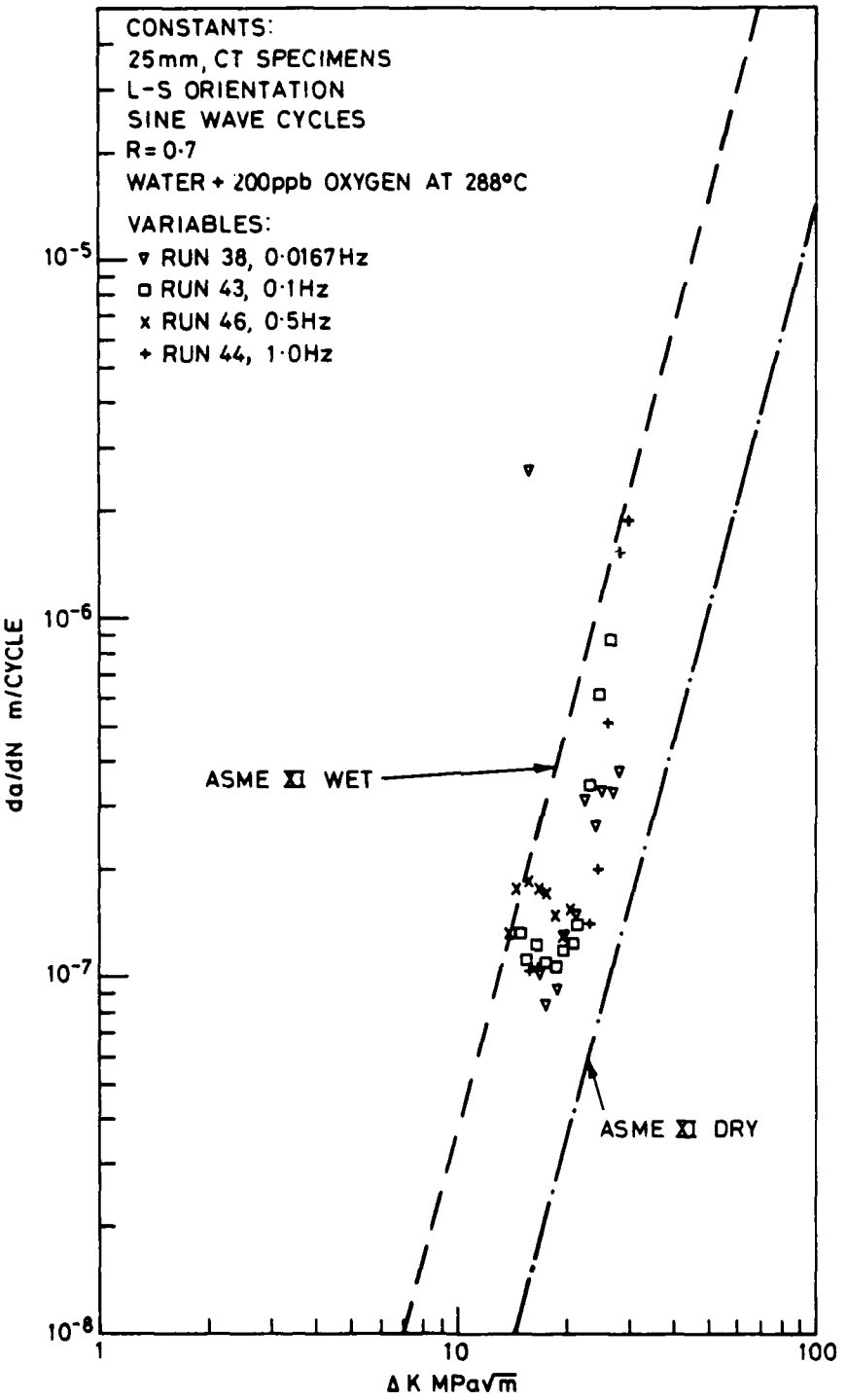

AERE - R 10201 Fig. 8

Influence of frequency on crack propagation rates in A533–B steel immersed in water plus 200 ppb oxygen at 288°C

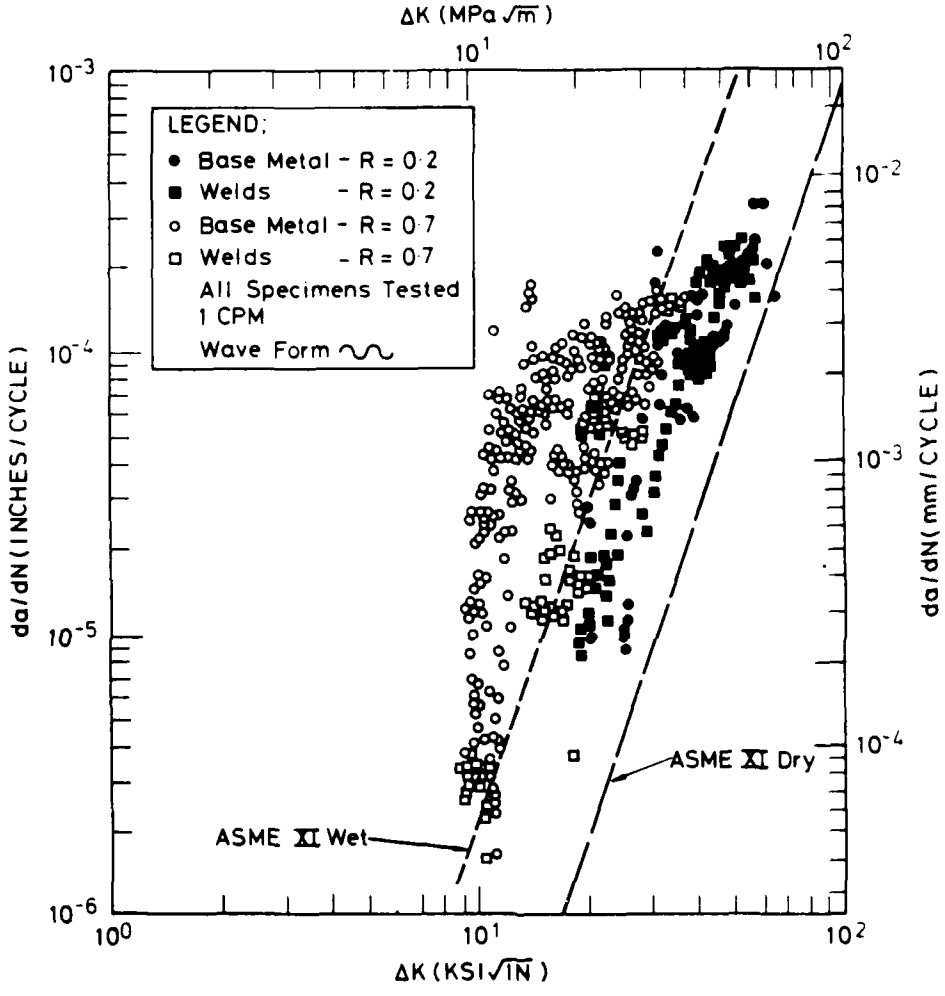

AERE - R 10201 Fig. 9

Corrosion fatigue data for A533–B–1 and A508–2 base metals and weldments in PWR primary water[7]

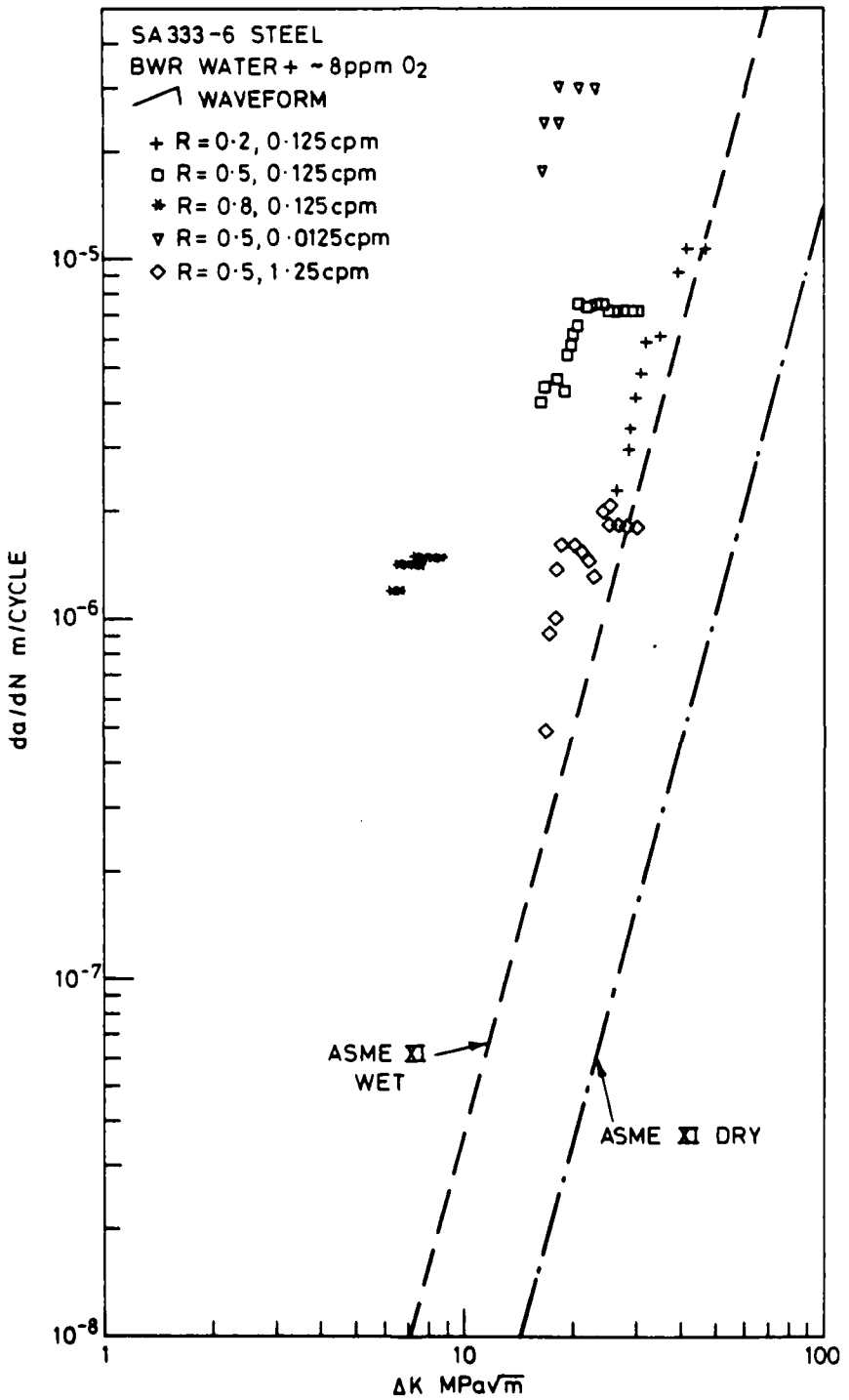

AERE - R 10201 Fig. 10
Corrosion fatigue data for SA333-6 steel in air saturated water at 288°C[11]

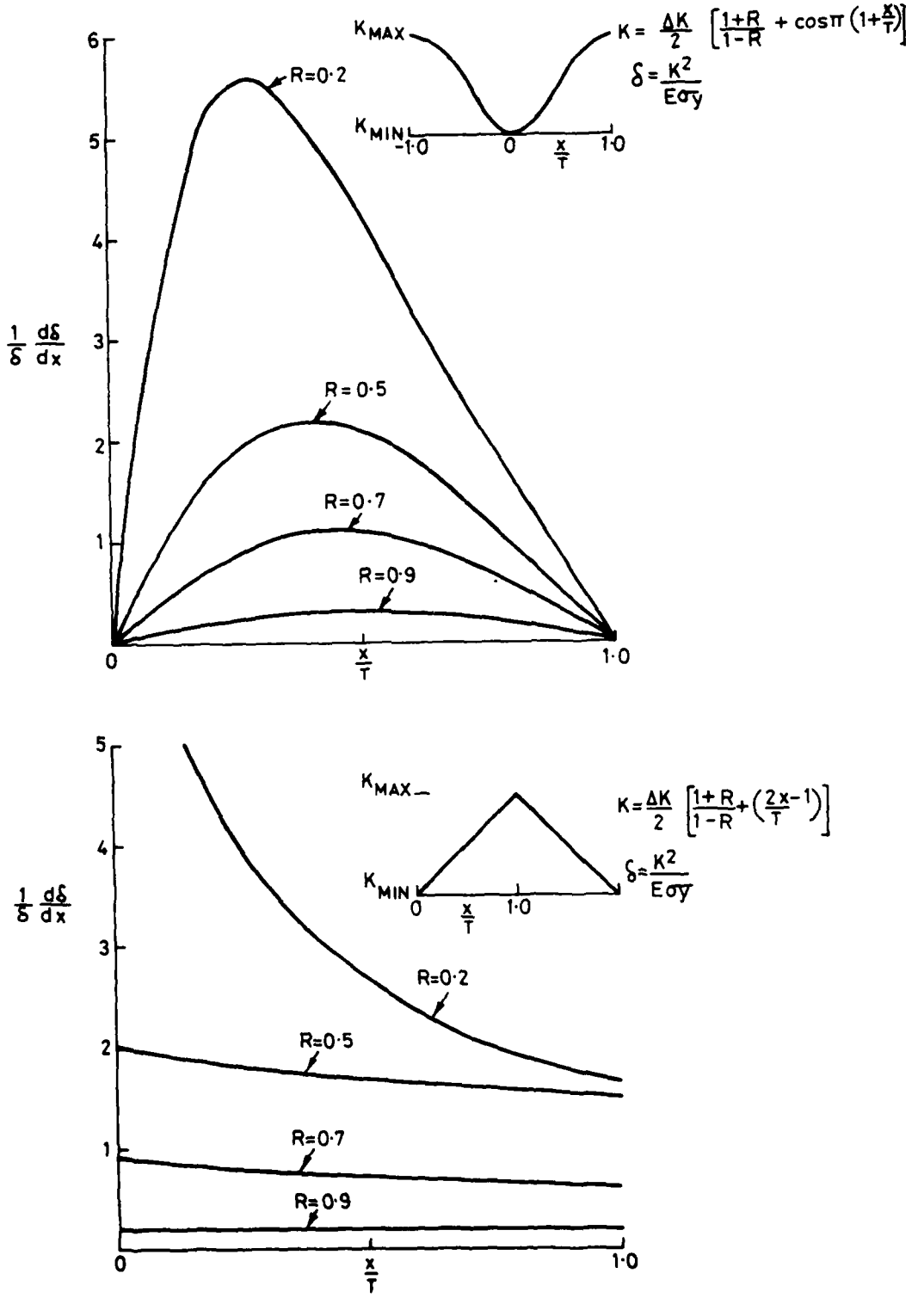

AERE - R 10201 Fig. 11
Crack tip strain rates during sine and triangle fatigue cycles

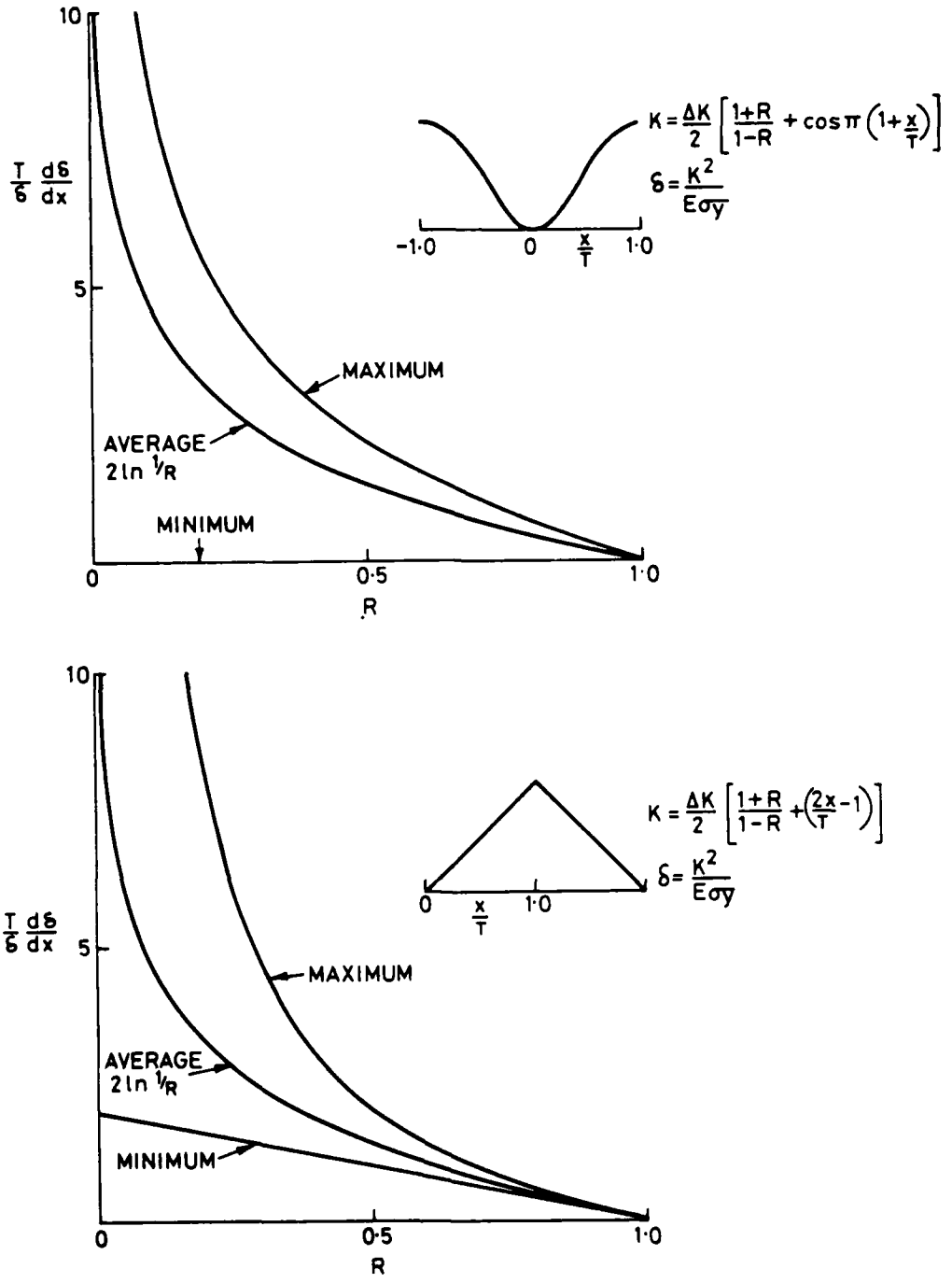

AERE - R 10201 Fig. 12

Average and maximum and minimum crack tip strain rates during sine and triangle fatigue cycles as a function of stress ratio

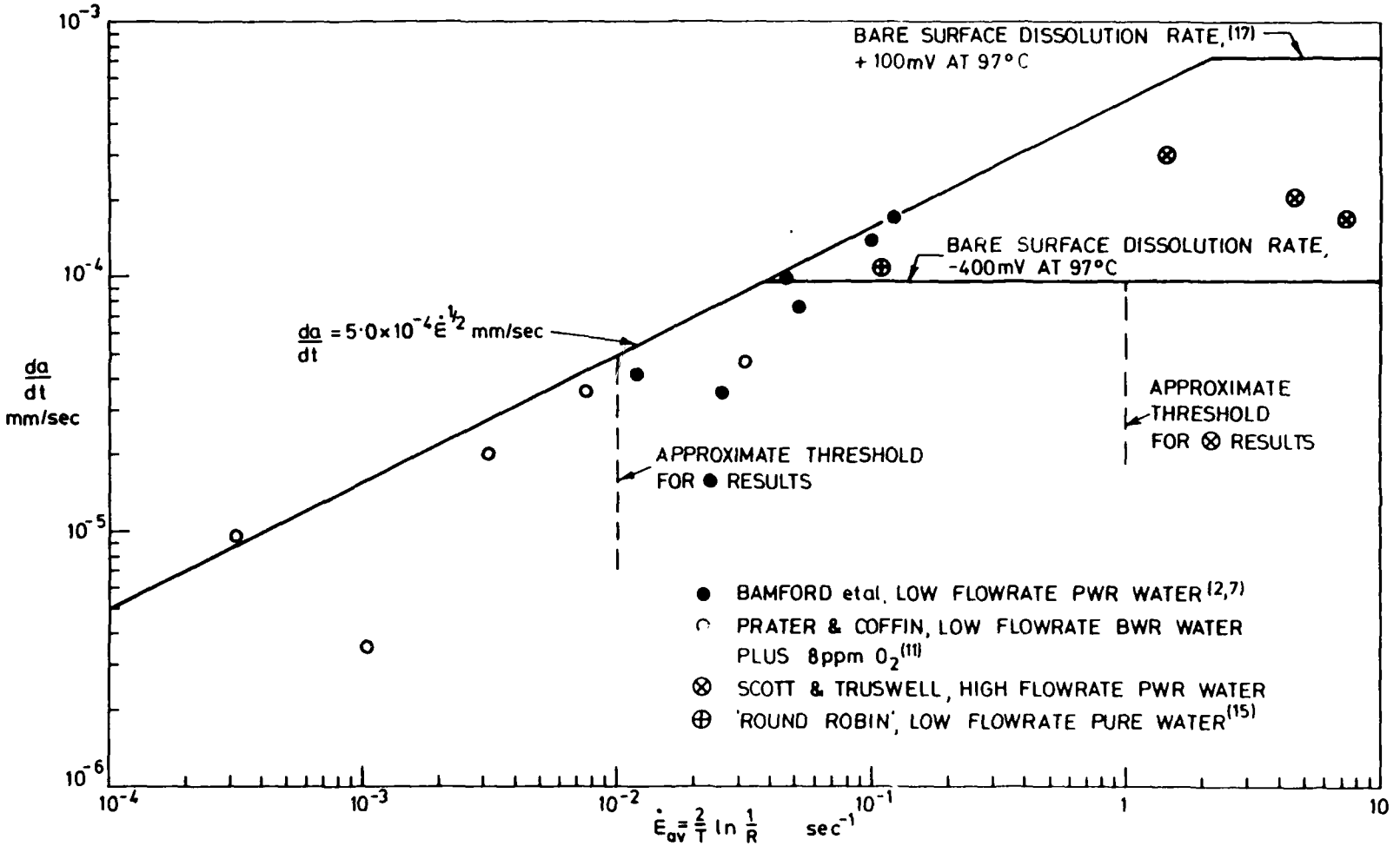

AERE - R 10201 Fig. 13
Plateau rates of crack growth as a function of crack tip strain rate

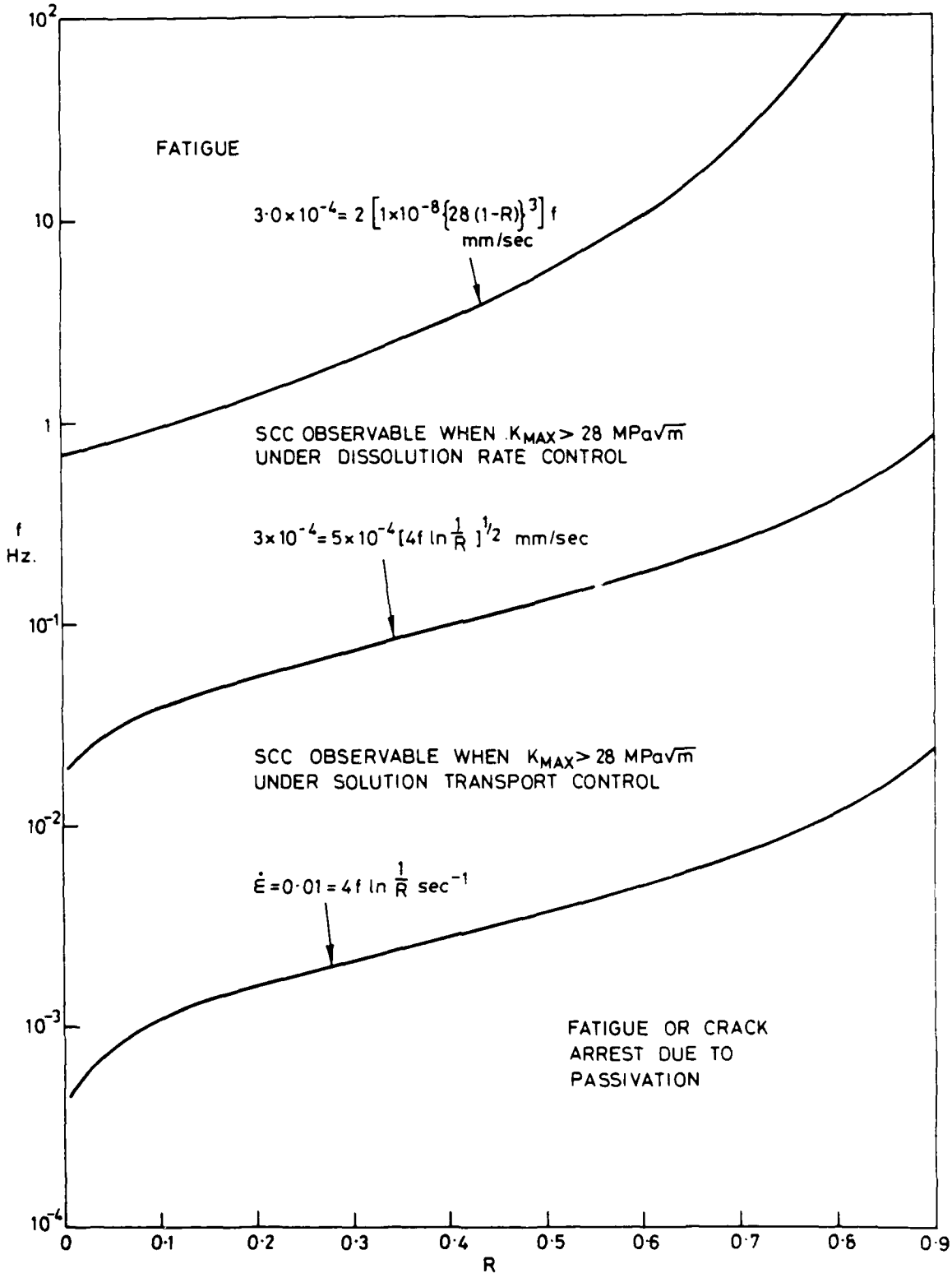

AERE - R 10201 Fig. 14

Combinations of frequency and stress ratio for which strain rate controlled stress corrosion cracking can be observed

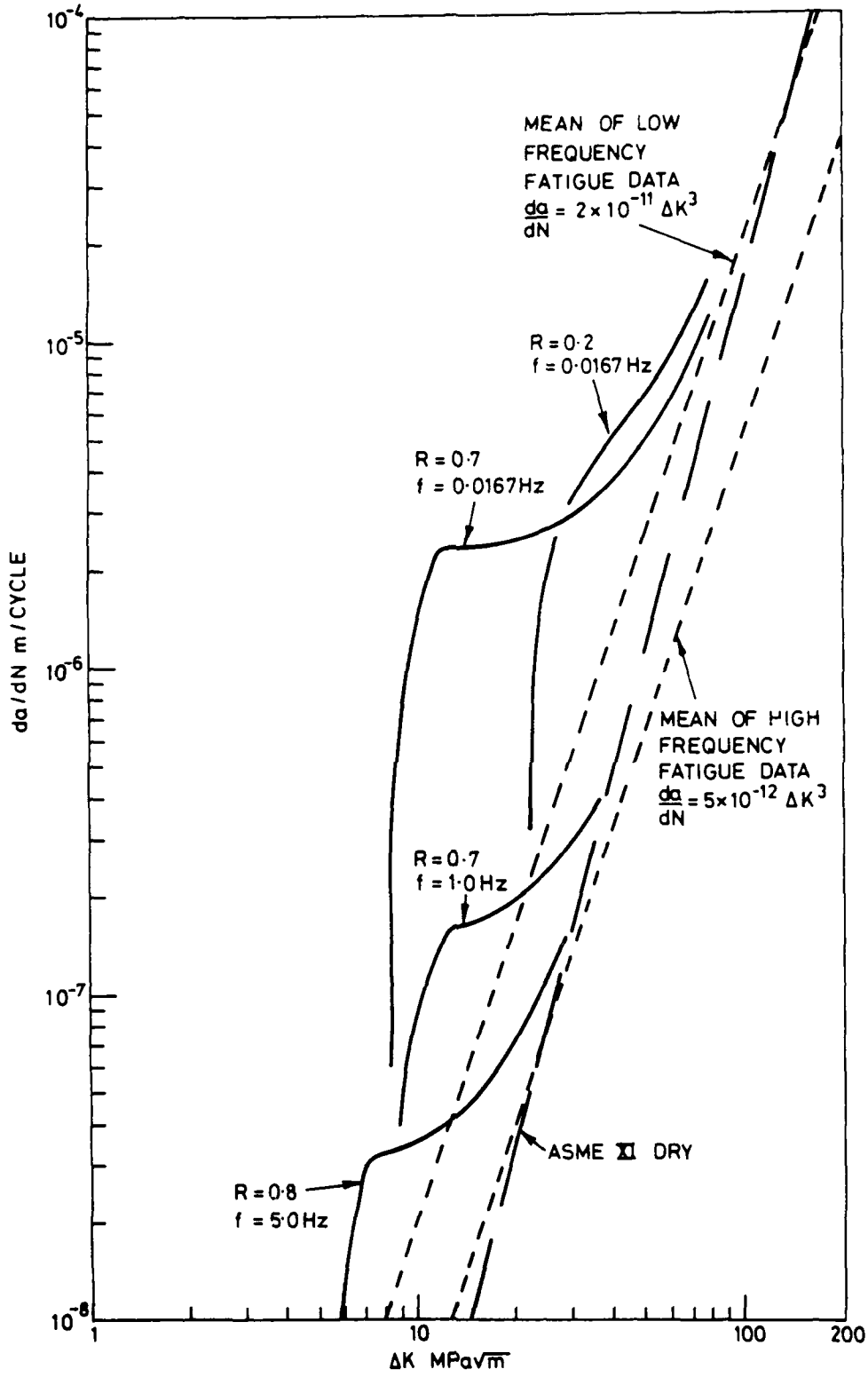

AERE - R 10201 Fig. 15
Calculated corrosion fatigue crack propagation curves including strain rate sensitive stress corrosion cracking

NOTE

To be published by the International Atomic Energy Agency as part of the Proceedings of a Specialist Meeting on Corrosion Fatigue held at Freiburg, 13-15 May, 1981.